

Learning Similarity between Scene Graphs and Images with Transformers

Yuren Cong¹, Wentong Liao¹, Bodo Rosenhahn¹, Michael Ying Yang²
¹TNT, Leibniz University Hannover, ²SUG, University of Twente

Abstract

Scene graph generation is conventionally evaluated by (mean) Recall@K, which measures the ratio of correctly predicted triplets that appear in the ground truth. However, such triplet-oriented metrics cannot capture the global semantic information of scene graphs, and measure the similarity between images and generated scene graphs. The usability of scene graphs is therefore limited in downstream tasks. To address this issue, a framework that can measure the similarity of scene graphs and images is urgently required. Motivated by the successful application of Contrastive Language-Image Pre-training (CLIP), we propose a novel contrastive learning framework consisting of a graph Transformer and an image Transformer to align scene graphs and their corresponding images in the shared latent space. To enable the graph Transformer to comprehend the scene graph structure and extract representative features, we introduce a graph serialization technique that transforms a scene graph into a sequence with structural encoding. Based on our framework, we introduce R-Precision measuring image retrieval accuracy as a new evaluation metric for scene graph generation and establish new benchmarks for the Visual Genome and Open Images datasets. A series of experiments are further conducted to demonstrate the effectiveness of the graph Transformer, which shows great potential as a scene graph encoder. Project page at <https://yrcong.github.io/gicon/>.

1. Introduction

A scene graph is a graphical representation in which nodes symbolize the entities in a scene and the edges indicate the relationships between the entities [18]. It is viewed as a potential approach to access comprehensive scene understanding, as well as a promising means to bridge the domains of vision and language. In recent years, the task of scene graph generation has received increasing attention, as it enables the automatic inference of complex graph information from images that can otherwise be costly to annotate manually. Many recent works have successfully explored


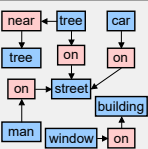
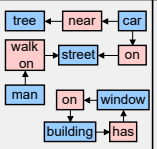
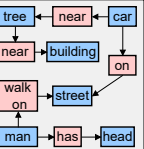
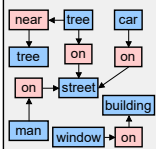



			
Recall@5	1.00	0.40	0.20
similarity	0.65	0.60	0.56
			
similarity	0.65	0.17	0.10

Figure 1: Our framework can quantitatively measure the similarity between scene graphs and images precisely. In the first row, even though each scene graph consists of different triplets, they describe semantically similar scenes and have high similarity to the image. In contrast, Recall@5 of these scene graphs differs significantly. The examples in the second row demonstrate our method can distinguish the semantic difference between scene graphs and scenes.

the potential of applying scene graphs in many vision tasks, such as image retrieval [18, 35, 50, 42], image generation [17, 26, 13, 47], image captioning [10, 49], and visual question answering [36, 22, 14].

Compared to the flourishing progress for generating high-quality scene graphs [51, 45, 27, 25, 38, 4, 5, 48], the risk related to scene graph evaluation is often overlooked. Almost all existing works apply the evaluation metrics of Recall@K and mean Recall@K, which are triplet-oriented and compare the predicted triplets with ground truth triplets. However, when the ground truth triplets are biased or noisy, such evaluation easily fails to reveal the true quality of the generated scene graphs. For example, consider a street scene in Fig. 1, where the scene graph is restricted to include only two nodes and one edge, *i.e.*, a triplet. If the predicted triplet is <man-walking on-street>, while the ground truth label is <man-on-street>, the widely-used evaluation metric Recall@K would be 0 due to bias. The risk is still ubiquitous when scene graphs are scaled

up. Such triplet-oriented evaluation metrics can limit the development of scene graphs and their application in downstream language-vision tasks. To overcome these limitations, a graph-oriented metric is urgently required to measure how well the global semantic information of a scene graph matches the visual appearance of the given image.

Multi-modal similarity [32] is a promising solution to determine the quality of generated scene graphs by calculating the distance between the scene graphs and the images in the shared latent space. To this end, we propose a simple contrastive learning framework for connecting scene graphs and images (**GICON**) and learning their similarity, as depicted in Fig. 1. Contrastive Language-Image Pre-training (CLIP) [34] has achieved impressive results in various language-vision tasks, inspiring us to adopt Transformers [41] as the encoders in our contrastive learning framework which is able to measure the similarity between scene graphs and images. Since Transformer cannot process graphical data directly, we propose a graph serialization technique that transforms a scene graph into a sequence and structural encoding.

To validate the rationality of the similarity measured by our framework, we introduce R-Precision which measures the image retrieval accuracy using generated scene graph as the new evaluation metric, which has been adopted in the task of text-to-image generation [44, 33]. Compared with triplet-oriented metrics, our graph-oriented metric is more robust against data bias and noise. Our **main contributions** are summarized as follows:

- We propose a simple yet effective contrastive learning framework based on Transformers to learn the similarity between scene graphs and images.
- The proposed graph serialization method enables our graph Transformer to comprehend the graph structure. It can be used as a generic scene graph encoder.
- A novel metric R-Precision based on our framework is introduced to evaluate scene graph generation by using the similarity between scene graphs and images.
- We create new benchmarks on Visual Genome [20] and Open Images [21], and perform a systematic analysis of the existing scene graph generation methods.

2. Related Work

Scene graphs. A scene graph is a structural and semantic description of a scene, which represents objects (as well as their attributes) as nodes and pairwise relationships as edges [18, 20, 16]. It has been shown to be promising for other vision tasks like image retrieval [18, 50], image captioning [49], image generation [17, 26, 47], and visual question answering [36, 22, 14]. A precise alignment between scene

graphs and images is crucial for these applications. In [18], a conditional random field is constructed to model the distribution over all possible scene graph groundings, and the likelihood of maximum a posterior inference is taken as the score measuring the similarity between the scene graph and the image. Yoon *et al.* [50] use scene graphs as the medium for image-to-image retrieval by measuring the similarity between scene graphs of images rather than between query scene graphs and images. For image captioning, Tang *et al.* [49] propose an encoder-decoder framework wherein a dictionary is learned to encode the language inductive bias from scene graphs to natural language sentences. The above methods usually use manually labeled scene graphs, which are costly to annotate. As a result, a large number of scene graph generation models have emerged [46, 11, 31, 23, 9]. Nevertheless, the consistency between the generated scene graph and the image is unknown. Recall@K is the most widely adopted metric to measure the performance of scene graph generators [30, 43, 51]. However, Recall@K crudely compares the predicted triplets with the ground truth relationships, which makes it sensitive to noise and bias in the dataset. In addition, Recall@K and other triplet-oriented metrics have no way to directly compare the consistency between generated scene graphs and images. To synthesize images, Johnson *et al.* [17] applies a graph convolutional network (GCN) to extract semantic information from the scene graph to predict the segmentation masks and the scene layout. To predict the layout as the semantic masks from scene graphs for image generation become the main paradigm for this task [13, 1, 26]. Nonetheless the improvements of these works by introducing scene graphs, an important factor is ignored: how to measure the similarities between the scene graphs and images. In this work, we fill this gap by proposing a contrastive learning framework, which can precisely compute the similarity between scene graphs and images.

Multi-modal contrastive learning. Contrastive learning is a discriminative representation learning which aims to group similar samples closer and diverse samples far from each other [15]. It plays an important role in self-supervised learning which is promising to handle the limitations of supervised learning that requires high-quality but expensive annotations. ConVIRT is proposed in [53] to learn medical visual representations by exploiting naturally occurring paired descriptive text. Desai *et al.* [7] use textual annotations of images on COCO Captions [3] to learn visual representations and achieve competitive performance to supervised and self-supervised learning methods. To make use of the myriad available images with textual descriptions, the recent work CLIP [34] pre-trained a visual-language model with the contrastive loss using 400 million image-text pairs collected from a variety of publicly available sources. Its pre-trained image encoder and text encoder have powerful

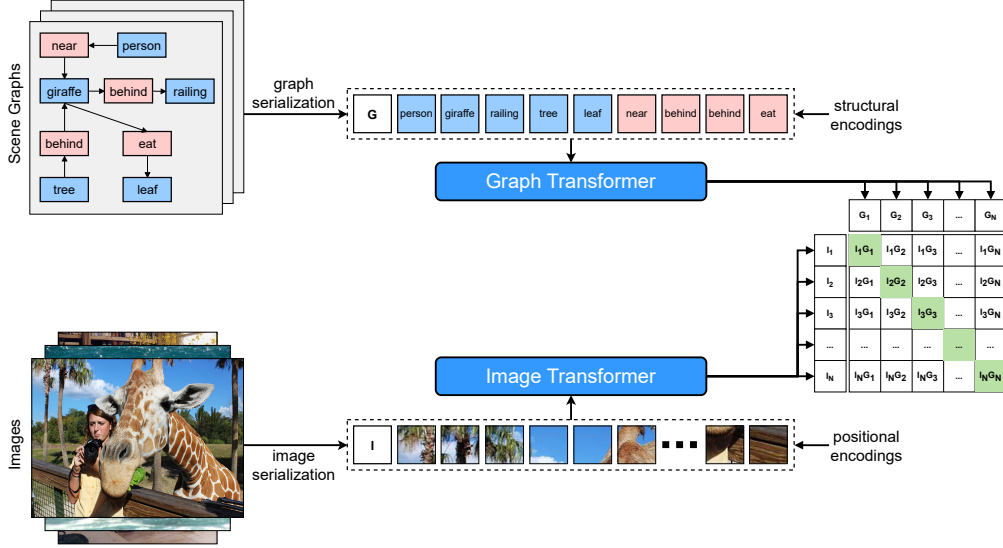


Figure 2: Overview of our method: **GICON** is a simple yet effective contrastive framework approach that involves a scene graph Transformer and an image Transformer to reason about scene graph and image representations, respectively. We use a contrastive loss to align the scene graph and its corresponding image in the shared latent space.

representations and have been successfully applied in many vision, language, and visual-language tasks. Contrastive learning is firstly used for scene graph generation in [52] to solve the entity instance confusion and the proximal relationship ambiguity issues. Yang *et al.* [47] train a scene graph GCN encoder with image-masked autoencoding loss, and then use it for the task of image generation from scene graphs.

Compare to the rapid development of visual and language representation learning, the representational learning for scene graphs is still far under explored. As we see that extracting powerful scene graph representations is the key to different tasks. Conventionally, GCNs [19] are popular choices for encoding scene graphs [26, 42, 13, 47]. However, GCNs are primarily designed to operate on local neighborhoods of nodes, which makes them less effective at capturing global representations. In this work, we propose a contrastive learning framework based on Transformers which is able to extract powerful representations for scene graphs and images. To the best of our knowledge, we are the first for this task.

3. Scene Graph-Image Contrastive Learning

In this paper, we propose a straightforward and robust contrastive learning framework to connect scene graphs and images (**GICON**). It consists of a scene graph encoder and an image encoder, both of which are built on the Transformer architecture [41]. The overview of our framework is demonstrated in Fig. 2. The input scene graph can be a location-free scene graph (where nodes only represent entity categories) or a location-bound scene graph (where

nodes represent entity categories and bounding boxes).

3.1. Scene Graph Representation

To use the Transformer for the graph-structured data, we propose a novel approach to serialize scene graphs and capture representative scene graph features using a Transformer. Given a scene graph with M entity nodes and N edges for the relationships, a scene graph sequence is constructed by concatenating node representations $\{\mathbf{n}_1, \mathbf{n}_2, \dots, \mathbf{n}_M\}$ and edge representations $\{\mathbf{e}_1, \mathbf{e}_2, \dots, \mathbf{e}_N\}$. For location-free scene graphs, $\mathbf{n} \in \mathbb{R}^d$ is used as the semantic embedding corresponding to the entity category. For location-bound scene graphs, we embed the bounding box information $\mathbf{b} \in \mathbb{R}^4$ using linear transformation layers. Then, the box embedding is element-wise added to the corresponding node representation.

As the above serialized scene graph sequence does not inherently capture the structural properties, we incorporate structural encoding within the sequence to enable the Transformer to understand the graph structure. We first construct M learnable node structural encodings $\{\mathbf{E}_1^n, \mathbf{E}_2^n, \dots, \mathbf{E}_M^n\}$ to differentiate the M nodes within a scene graph, and utilize the node encodings to determine the edge structural encodings $\{\mathbf{E}_1^e, \mathbf{E}_2^e, \dots, \mathbf{E}_N^e\}$ (see Fig. 3). Concretely, for the edge \mathbf{e}_k from the start node \mathbf{n}_i to the end node \mathbf{n}_j , the edge encoding is computed as $\mathbf{E}_k^e = \mathbf{E}_i^n - \mathbf{E}_j^n$, which preserves the relation direction between entities. The graph sequence S_G and structural encoding E_G can be formulated as:

$$\begin{aligned} S_G &= [\mathbf{n}_1, \mathbf{n}_2, \dots, \mathbf{n}_M, \mathbf{e}_1, \mathbf{e}_2, \dots, \mathbf{e}_N] \\ E_G &= [\mathbf{E}_1^n, \mathbf{E}_2^n, \dots, \mathbf{E}_M^n, \mathbf{E}_1^e, \mathbf{E}_2^e, \dots, \mathbf{E}_N^e]. \end{aligned} \quad (1)$$

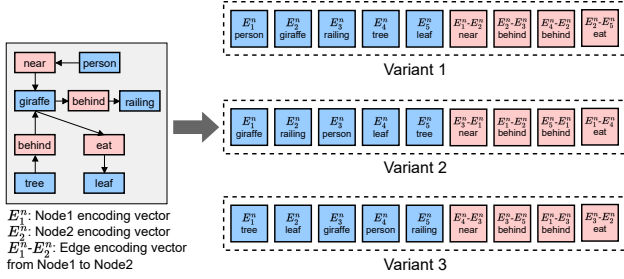


Figure 3: We introduce a graph serialization technique to convert a scene graph into a graph sequence and structural encodings. To prevent node encodings from over-memorizing the absolute order, we randomly shuffle the nodes and assign them different structural encodings during each iteration.

The node position within the scene graph is determined by its relationship to other nodes, making it relative rather than absolute. To prevent node encodings from over-memorizing the absolute order, nodes are shuffled in graph serialization. Specifically, we shuffle nodes from the same graph and assign them different node encodings during different iterations of training. The serialization outcome for the same graph varies, and the node encodings are encouraged to learn robust structural information of scene graphs.

To learn scene graph representations, we use the vanilla Transformer encoder stack [41]. Each encoder layer consists of a multi-head attention module, a feed-forward network, and normalization layers. Similar to the [class] token in BERT [8], a learnable graph embedding $\mathbf{g} \in \mathbb{R}^d$ is constructed and inserted into the graph sequence to extract the scene graph representation. No additional encoding is preserved. In the multi-head attention module, the structural encoding E_G is added to the scene graph sequence S_G to construct the query and key while the value is S_G directly. The graph embedding \mathbf{g} from the last encoder layer is used as the final scene graph representation.

3.2. Image Representation

Inspired by DETR [2], we learn image representations with a Transformer while keeping the original aspect ratio of the input images. For image pre-processing, we do not perform image cropping, which will decrease the consistency between the scene graph and the image.

We use a ResNet-50 [12] to extract the feature map, and a convolution layer to transform the channel dimension of the feature map to the model dimension d . To make the batch operation feasible, the images with different sizes in the batch are zero-padded to the same shape of $L \times L \times 3$, as depicted in Fig. 4. Then, the feature maps are serialized into a feature sequence of length L^2 . The features of the zero-padded patches are masked off in the image Transformer.

Similar to the graph encoder, we adopt the vanilla Trans-



Figure 4: In order to maintain consistency between scene graphs and images, input images with different aspect ratios in the batch are zero-padded to a square of length L , rather than being cropped and resized. As a result, the length of resultant sequences is L^2 . Zero-padded patches are masked off in the image Transformer.

former encoder stack to learn image representations. To capture the image representation, we also construct a learnable image embedding $\mathbf{i} \in \mathbb{R}^d$ and incorporate it into the feature sequence. As the Transformer architecture is permutation-invariant, fixed positional encodings [41, 2] are introduced to facilitate the recognition of the relative positions and spatial layout of the features. The image embedding \mathbf{i} from the last Transformer layer is used as the final image representation.

3.3. Objective Function

To align the scene graph and corresponding image in the shared latent representation space, we adopt the contrastive loss as the optimization objective. Given a batch of B scene graph-image pairs, the loss function is formulated as:

$$L = -\frac{1}{B} \sum_{i=1}^B \left(\log \frac{\exp(\text{sim}(\mathbf{g}_i, \mathbf{i}_i))}{\sum_{j=1}^N \exp(\text{sim}(\mathbf{g}_i, \mathbf{i}_j))} + \log \frac{\exp(\text{sim}(\mathbf{g}_i, \mathbf{i}_i))}{\sum_{j=1}^N \exp(\text{sim}(\mathbf{g}_j, \mathbf{i}_i))} \right), \quad (2)$$

where $\text{sim}(\mathbf{g}_i, \mathbf{i}_j)$ indicates the cosine similarity between the i -th scene graph representation \mathbf{g}_i and the j -th image representation \mathbf{i}_j in a batch. The first term in Eq. 2 aims to increase the similarity between the scene graph and its corresponding image compared to other images while the second term increases the similarity between the image and its corresponding scene graph compared to other scene graphs.

4. Evaluation for Scene Graph Generation

We review the commonly used evaluation metrics for scene graph generation (SGG) and their limitations. Then, we propose using R-Precision based on GICON to evaluate the quality of generated scene graphs.

Recall@K and mean Recall@K. Recall@K is first in-

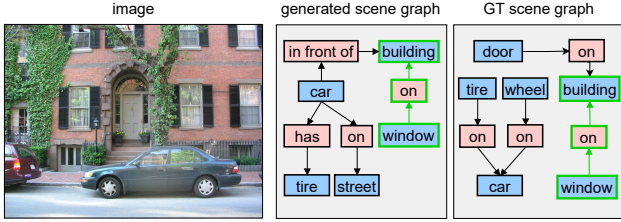


Figure 5: The commonly used Recall@K is sensitive to the bias in the ground truth. The generated scene graph is highly representative. However, the recall value is low since only `<window-on-building>` is included in the biased ground truth graph (highlighted in green).

roduced for visual relationship detection (VRD) [30] and is further widely used to evaluate SGG methods. It calculates the fraction of ground truth triplets that appear in the top K confident triplet predictions. Due to the long tail issue in the scene graph dataset such as Visual Genome [20], mean Recall@K is proposed to evaluate the inference performance of SGG models for low-frequency predicates [39]. It computes the recall on each predicate category independently and takes their average. However, both Recall@K and mean Recall@K have limitations, as they critically compare the predicted triplet set with the ground truth triplet set and are thus sensitive to noise and bias in the dataset annotations, as illustrated in Fig. 5.

Weighted mAP. mAP_{rel} evaluates the mean average precision of the relationships where the subject and object boxes have an IOU of at least 0.5 with ground truth, while mAP_{phr} is designed for the enclosing relationship box. They are used for VRD evaluation in the Open Images [21] Challenge. $wmAP_{rel}$ and $wmAP_{phr}$ are proposed for more class-balanced evaluation [52]. The weighted mAP is also triplet-oriented and therefore has the same limitations as Recall@K and mean Recall@K.

R-Precision. The better a scene graph describes an image, their alignment is closer in the shared latent space. To this end, we propose a novel evaluation metric R-Precision based on GICON for scene graph generation evaluation. R-Precision measures the retrieval accuracy when retrieving the matching image from K image candidates using the generated scene graph as a query. We use the scene graph and image representations provided by GICON to compute the scene graph-image similarity score for retrieval. A larger K implies that the retrieval task is more challenging, and the query scene graph’s quality demands are higher. Our new metric can evaluate both location-free scene graphs and location-bound scene graphs. In contrast to triplet-oriented metrics, R-Precision based on GICON compares the semantic context and visual appearance, therefore, it is more robust to the perturbation of single triplets.

5. Experiments

5.1. Datasets

The experiments are conducted on two benchmark datasets for scene graph generation, Visual Genome [20] and Open Images V6 [21]. We establish new benchmarks with our graph-oriented metrics for both datasets.

Visual Genome. For the Visual Genome dataset, we follow the data split from [43], which is adopted by most scene graph generation methods. There are 108k images in the dataset with 150 entity categories and 50 predicate categories. In the task of scene graph generation, 70% of the images are used for training while the remaining 30% are used for evaluation.

Open Images V6. Recently, an increasing number of scene graph generation methods are validated on Open Images. The large-scale Open Images V6 has 126k training images and 5.3k test images with 300 entity categories and 30 predicate categories.

5.2. Technical Details

We adopt the same setting for training on both of the Visual Genome and Open Images V6 datasets. We train our framework using an AdamW optimizer [29] with a learning rate of $1e^{-4}$ on 8 GPUs with a batch size of 32 per GPU. The model dimension d for both the graph Transformer and image Transformer is set to 512, allowing for the calculation of similarity between scene graphs and images. If not otherwise specified, the default number of layers for the graph Transformer and the image Transformer is 6. The length of the learnable node structural encodings is restricted to 10. If a scene graph contains more than 10 entity nodes, we randomly sample 10 nodes and clip the others. The input image is scaled, with the longest side being 512, and is zero-padded into a square. For both datasets, only the training set is used in the contrastive training. More details are provided in the supplementary material.

5.3. Scene Graph Generation Benchmarks

Considering that the triplet-oriented metrics cannot directly reflect the consistency between generated scene graphs and images, we re-evaluate the prior scene graph generation models with the graph-oriented metric R-Precision ($K= 10/50/100$) based on the similarity computed by GICON. We create two benchmarks, respectively for the Visual Genome and Open Images V6 datasets, and perform a systematic analysis. Different from triplet-oriented metrics, which require bounding box information to calculate IoU, the new metric is also applicable to location-free scene graphs and provides a reference for semantic downstream tasks. Despite the large amount works for scene graph generation, we only evaluate a selection of

Method		SGDET				R-Precision (LF Graph)			R-Precision (LB Graph)			Year
		R@20	R@50	mR@20	mR@50	K=10	K=50	K=100	K=10	K=50	K=100	
Ground Truth		-	-	-	-	86.7	67.9	58.0	92.1	78.9	71.0	-
two-stage	MOTIFS [51]	21.4	27.2	<u>4.1</u>	<u>5.7</u>	84.5	65.1	54.9	90.2	74.5	69.1	2018
	ReIDN [52]	21.1	28.3	<u>4.9</u>	<u>6.4</u>	88.9	72.5	62.7	93.5	83.1	75.0	2019
	NODIS [5]	21.6	27.7	<u>5.1</u>	<u>6.0</u>	85.0	66.9	58.1	90.5	75.6	69.8	2020
	MOTIFS-TDE [38]	12.4	16.9	<u>5.8</u>	<u>8.2</u>	94.5	82.9	74.7	97.8	91.8	87.1	2020
	VCTree-EBM [37]	24.2	31.4	5.7	7.7	92.9	78.0	68.9	96.5	87.7	81.7	2021
	BGNN [25]	<u>23.3</u>	31.0	7.5	10.7	93.3	79.4	70.9	97.1	89.7	84.3	2021
one-stage	FCSGG [28]	16.1	21.3	2.7	3.6	79.0	59.2	49.8	87.4	70.1	66.7	2021
	SGTR [24]	<u>19.5</u>	24.6	7.5	12.0	94.5	83.1	74.9	97.3	90.8	85.7	2022
	ReITR [6]	21.2	27.5	6.8	10.8	93.1	80.1	71.1	97.0	90.1	84.8	2022
	SSR-CNN [40]	25.8	32.7	6.1	8.4	91.6	74.4	64.0	95.9	86.5	79.6	2022

Table 1: Benchmarking different scene graph generation models on the Visual Genome dataset. We re-evaluate 6 two-stage methods and 4 one-stage methods using R-Precision (K=10/50/100) for location-free scene graphs (LF Graph) and location-bound scene graphs (LB Graph). The highest score in each column is in **bold**. The underlined numbers indicate that the scores are not published in the original papers, but are re-evaluated.

representative models for which official code and trained weights are available due to limited computation resources.

Visual Genome Benchmark. We benchmark 6 two-stage SGG methods [51, 52, 5, 38, 37, 25] and 4 one-stage SGG methods [28, 24, 6, 40] for Visual Genome. The evaluation scores are given in Tab. 1. For both location-free scene graphs and location-bound scene graphs, we are surprised to find that R-Precision of most methods is higher than R-Precision using ground truth scene graphs (first row in Tab. 1). For location-free scene graphs, the R-Precision (K=100) of SGTR [24] is 16.9 higher than the ground truth, and for location-bound scene graphs, the R-Precision (K=100) of MOTIFS-TDE [38] is 16.1 higher than the ground truth. This demonstrates that the scene graphs generated by the existing models have higher similarity to the corresponding images than manually labeled scene graphs and perform better in the task of image retrieval. We conjecture that the main reasons for the phenomenon are as follows:

- The manual annotations of Visual Genome are noisy and incomplete. Some ground truth scene graphs consist of only one or two relationships, while generated scene graphs always include several triplets.
- Bias in ground truth scene graphs has already received attention. Many models can generate unbiased scene graphs from biased training, which makes the information in scene graphs more diverse.

Moreover, we find that R-precision is not linearly correlated with the previous triplet-oriented evaluation metrics (see Fig. 6). The unbiased model MOTIFS-TDE does not perform better than some other SGG methods in terms of mean Recall@K, and has the lowest Recall@K while it reports the best R-Precision performances for both location-free scene graphs and location-bound scene graphs. From

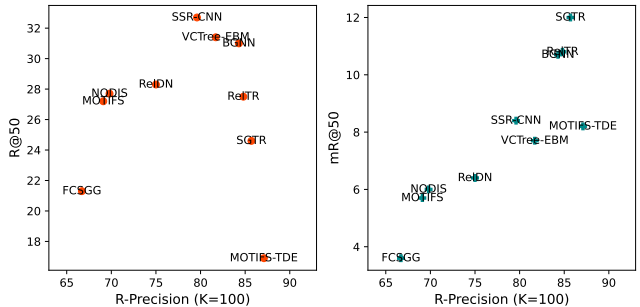


Figure 6: R@50, mR@50 and R-precision (K=100) scores of different SGG models on the Visual Genome dataset for location-bound scene graphs.

the results, usually the higher mean Recall@K of the model, the higher its R-precision score.

Open Images V6 Benchmark. We benchmark 4 SGG methods [25, 24, 6, 40] for the Open Images V6 dataset. The evaluation scores are shown in Tab. 2, where score_{wtd} indicates the weighted score = 0.2×R@50+0.4×wmAP_{rel}+0.4×wmAP_{phr}. The R-Precision scores using ground truth scene graphs for retrieval on the Open Images dataset are similar to Visual Genome. The R-Precision (K=100) is 55.4 for location-free scene graphs and 73.4 for location-bound scene graphs. We also observe that the SGG models do not achieve the same level of performance on Open Images as they do on Visual Genome, especially for location-free scene graphs. The reason for this can be that Open Images V6 has a different data distribution (e.g. more entity categories) and the optimization of SSG model hyperparameters is usually based on the Visual Genome dataset. For location-free scene graphs, SGTR has the best performance with R-Precision (K=100) of 46.3, which is 9.1 lower than using ground truth scene graphs. For location-bound scene

Method	R@50	wmAP _{rel}	wmAP _{phr}	score _{wtd}	R-Precision (LF Graph)			R-Precision (LB Graph)			Year
					K=10	K=50	K=100	K=10	K=50	K=100	
Ground Truth	-	-	-	-	89.2	67.5	55.4	94.2	82.0	73.4	-
BGNN [25]	75.0	33.5	34.2	41.7	72.3	43.1	32.6	91.5	75.6	66.8	2021
SGTR [24]	59.9	37.0	38.7	42.3	82.6	57.6	46.3	94.9	83.6	76.0	2022
RelTR [6]	71.7	34.2	37.5	43.0	79.9	55.0	42.1	93.9	82.1	75.2	2022
SSR-CNN [40]	76.7	53.3	43.6	49.4	77.7	53.3	40.9	95.9	85.6	78.7	2022

Table 2: Benchmarking different scene graph generation models on the Open Images V6 dataset. We re-evaluate 4 scene graph generation methods using R-Precision (K=10/50/100) for location-free scene graphs (LF Graph) and location-bound scene graphs (LB Graph). The highest score in each column is in **bold**.

Method	R-Precision (LF Graph)			R-Precision (LB Graph)		
	K=10	K=50	K=100	K=10	K=50	K=100
CLIP [34]	79.8	57.8	47.2	-	-	-
GICON-Node	78.9	56.6	46.4	84.2	70.8	64.6
GICON-Edge	12.1	3.4	1.8	-	-	-
GICON	86.7	67.9	58.0	92.1	78.9	71.0

Table 3: Quantitative results for image retrieval task using R-Precision as the evaluation metric. GICON-Node and GICON-Edge indicate only node embeddings or edge embeddings are given to compute the similarity, and the graph structure is artificially disrupted.

graphs, SSR-CNN outperforms the other methods with R-Precision (K=100) of 78.7, which is 5.3 higher than using ground truth scene graphs. Due to limited data, it is difficult to determine the correlation between R-Precision and $wmAP_{rel}/wmAP_{phr}$. However, for location-bound scene graphs, the higher the weighted mAP of the model, the higher its R-Precision score.

5.4. Image Retrieval with Similarity

To evaluate the effectiveness of our framework, we conduct image retrieval experiments using the similarity scores between ground truth scene graphs and images provided by GICON on the Visual Genome dataset.

We use scene graphs to retrieve the images without any additional annotations (e.g. object bounding boxes), which is different from other methods [18, 35]. Therefore, we first employ CLIP (ViT-B-32) [34] to establish a baseline. Considering that CLIP only encodes text, we concatenate the triplets in the scene graph into a string format and use the text as the query for image retrieval. More details are provided in the supplementary. Since CLIP does not incorporate bounding box information, we only test location-free scene graphs using this method. Furthermore, we conduct experiments to investigate the contribution of node and edge information in scene graphs to the image retrieval task. We use only node (GICON-Node) or edge (GICON-Edge) information as the query for image retrieval, and for both methods, the input graph structure is artificially disrupted. During training and evaluation, only node embeddings or

Method	R-Precision (LF Graph)			R-Precision (LB Graph)		
	K=10	K=50	K=100	K=10	K=50	K=100
GCN	78.9	57.9	46.2	84.5	70.9	63.2
Transformer (w/o Structural Encoding)	80.1	58.1	47.8	87.2	71.7	65.1
Transformer (w/o Node Shuffle)	83.4	62.4	52.8	89.4	75.0	68.3
Transformer (full)	86.7	67.9	58.0	92.1	78.9	71.0

Table 4: Ablation study on the graph Transformer. We compare the effectiveness between the Transformer and GCN. Moreover, we ablate structural encodings and node shuffle in graph serialization to analyze their impact.

edge embeddings are given.

The quantitative results are shown in Tab. 3. Compared to CLIP, GICON has significantly better R-Precision. In addition, GICON can retrieve images more accurately with the additional constraint of entity bounding boxes. Specifically, when using location-bound scene graphs as queries, the R-Precision (K=100) is 13.0 compared to location-free scene graphs. Comparing GICON-Node and GICON-Edge, we observed that node information, *i.e.*, the entities in the scene, play a dominant role in computing the similarity for image retrieval. The phenomena indicate that entities decide the main information of a visual scene. Adding the edge information helps understand the visual scene structurally and improves image retrieval performance.

The qualitative results are demonstrated in Fig. 7. The similarity values are not scaled or normalized. Our framework is capable of inferring reasonable similarities between images and both location-free and location-bound scene graphs, leading to successful image retrieval. Moreover, we observe that using location-bound scene graphs, which incorporate the constraint of entity bounding boxes, can better distinguish the visual scenes compared to using location-free scene graphs.

5.5. Ablation Study

We conduct experiments on the Visual Genome dataset to validate the effectiveness of the graph Transformer. Additionally, we investigate the impact of batch size on model performance.

Graph transformer. We compared the performance of the graph Transformer with that of a graph convolutional



Figure 7: Qualitative results for inferring similarity between scene graphs and images. Our framework can infer reasonable similarities between images and location-free as well as location-bound scene graphs. Matched scene graph and image are highlighted in green, and *entity** indicates the bounding box is given in the location-bound scene graph.

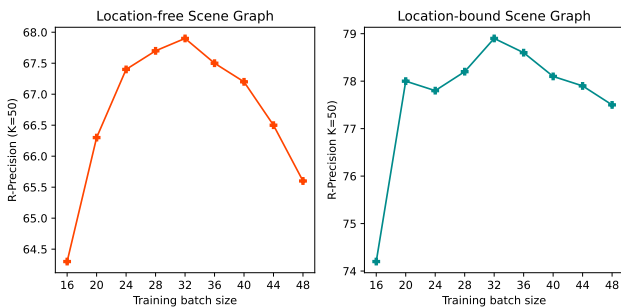


Figure 8: We perform experiments with different batch sizes to train our framework and finally adopt a batch size of 32.

network (GCN) with 6 layers [19]. Moreover, we conduct ablative experiments to analyze the impact of structural encodings and node shuffle in graph serialization. The results are demonstrated in Tab. 4. The graph Transformer outperforms the GCN for both location-free and location-bound scene graphs. However, without structural encoding, the graph Transformer is unable to comprehend the graph structure, resulting in a significant performance drop. In addition, we find node shuffle prevents node encodings from over-memorizing the absolute order, thus improving the overall performance.

Batch size. Batch size is a crucial factor that can significantly affect the effectiveness of contrastive learning. Therefore, we conduct experiments with different batch sizes using our framework and evaluate GICON based on R-Precision (K=50) as the evaluation metric. The results are depicted in Fig. 8, which indicate that using batch sizes between 20 and 40 yields similar results for both location-

free and location-bound scene graphs. The selection of a batch size that is too small or too large can lead to performance drops. Too large a batch size is likely to result in similar graph-image pairs in the batch. We finally adopt a batch size of 32 for training.

6. Conclusion and Future Work

In this paper, we propose a straightforward contrastive learning framework (GICON) based on Transformers that connects scene graphs and images. In order to use the Transformer to reason about scene graph representations, we introduce a graph serialization technique that transforms a scene graph into a sequence and structural encoding. Our framework enables the quantitative measurement of similarity between scene graphs and images. Based on that, a graph-oriented evaluation metric R-Precision is introduced for scene graph generation, which measures the image retrieval accuracy using the similarity between generated scene graphs and images. The new benchmarks are created for the Visual Genome and Open Images datasets with the new metric. We find the scene graphs generated by the advanced SGG models have higher similarity to the corresponding images than manually labeled scene graphs and perform better in the task of image retrieval. In addition, our graph Transformer can be used as a generic scene graph encoder for other downstream tasks. Although we do not use the output nodes and edge representations inferred from the graph Transformer in this work, decoding them for fine-grained learning is a promising direction for a number of related vision tasks.

Appendix

In this supplementary material, we first provide additional implementation details of our framework in Sec. A. More details about the similarity between scene graphs and images are discussed in Sec. B. In Sec. C, we show the additional ablation study. The additional qualitative results for image retrieval are presented in Sec. D.

A. Implementation Details

Node and edge representation We construct 150 entity embeddings as well as 50 predicate embeddings for Visual Genome [20], and 300 entity embeddings as well as 30 predicate embeddings for Open Images V6 [21]. They are learnable embeddings according to the entity or predicate categories. For a location-free scene graph, the node representations are the corresponding entity embeddings and the edge representations are the corresponding predicate embeddings. For a location-bound scene graph, the node representations are the corresponding entity embeddings element-wise added with the box embeddings, which are inferred from the bounding box coordinates.

Box embedding The box embedding has a dimension of 512, which is the same as the node representation. This allows the two to be element-wise added together. For a location-bound scene graph, the given bounding box coordinates $[x, y, w, h]$ of a node are transformed into a box embedding by linear transformation layers with normalization, as depicted in Fig. 9. The box embedding is then injected into the corresponding node representation as location information.

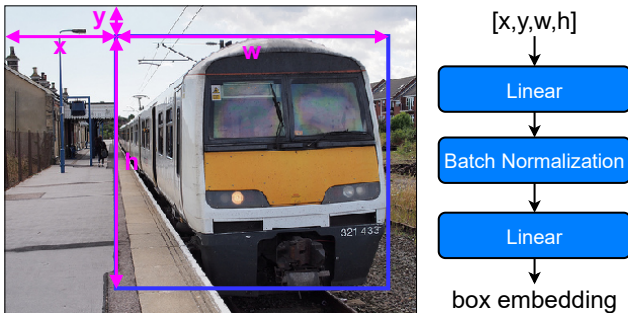


Figure 9: We convert the bounding box coordinates $[x, y, w, h]$ into the box embedding with linear layers with batch normalization, where x, y represent the coordinates of the upper left corner of the box, while w, h denote the width and height, respectively.

Graph serialization To enable the Transformer to handle a scene graph, we propose a graph serialization technique, where a scene graph is serialized to a sequence of node representations and edge representations. In order to retain the

structural information, we introduce structural encoding to represent the graphical structure, which is further used in the graph Transformer. An example of graph serialization is illustrated in Fig. 10. We first construct 10 learnable node structural encodings to distinguish different nodes in the scene graph. If a scene graph contains more than 10 entity nodes, we randomly sample 10 nodes and clip the others. If the number of nodes is less than 10, the redundant node encodings are not activated. The node encodings are randomly assigned to the nodes. In the given example, we view [person] as the first node and assign E_1^n to it. [giraffe] is viewed as the second node, and so on. The edge encoding indicates from which node the corresponding edge is directed to which node. For example, the edge encoding for [behind] from the second node [giraffe] to the third node [railing] is $E_2^n - E_3^n$. For another [behind] in the scene graph, the corresponding encoding is $E_4^n - E_2^n$, since it starts from the fourth node [tree] to the second node [giraffe]. To learn the graph representation, we insert a learnable graph embedding in the graph sequence but preserve no encoding for it.

Transformer architecture For both the graph Transformer and the image Transformer, we adopt the architecture of the vanilla Transformer encoder [41], which is shown in Fig. 11. Each Transformer layer consists of a multi-head attention module, a feed-forward network, and two Layer normalization. The graph embedding g and image embedding i from the last encoder layers are used as the final scene graph representation and image representation.

CLIP baseline for image retrieval For the task of image retrieval, we employ CLIP (ViT-B-32) [34] to establish a baseline. Since CLIP only supports text as input, we concatenate the triplets in the location-free scene graph into a string format (see Fig. 12). The converted text and images are respectively encoded by the CLIP text encoder and image encoder. The similarity between query text and image candidates is computed for image retrieval. Compared to CLIP, our framework GICON performs better, which uses location-free scene graphs as queries.

B. Similarity between scene graphs and images

We compute the cosine similarity between scene graphs and images:

$$\text{similarity} = \frac{\mathbf{g} \cdot \mathbf{i}}{\|\mathbf{g}\| \cdot \|\mathbf{i}\|}, \quad (3)$$

where \mathbf{g} and \mathbf{i} indicate the graph representation and image representation respectively. For the Visual Genome dataset, the maximum similarity between any location-free/location-bound scene graph and image in the test set is 0.79/0.78 and the minimum is -0.55/-0.59, while the average similarity between matched ground truth scene graphs

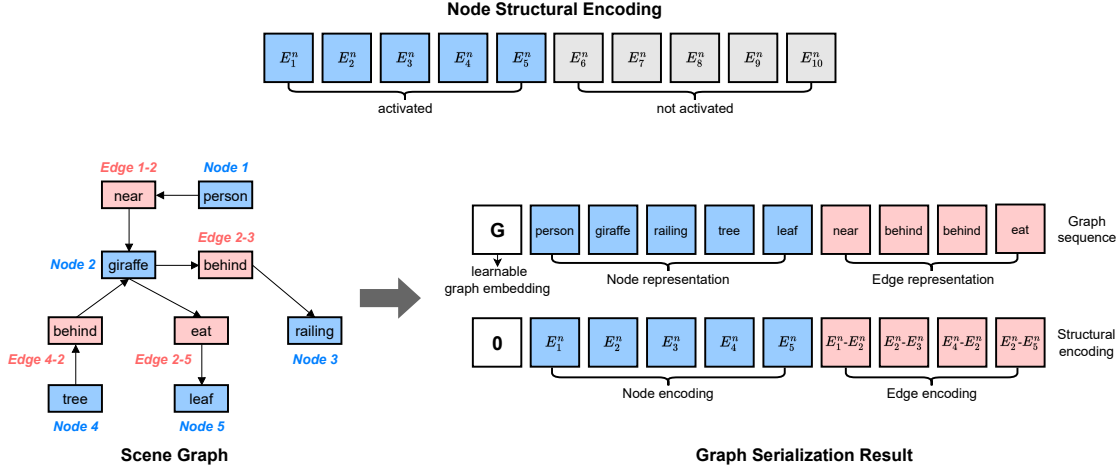


Figure 10: An example of graph serialization. The node structure encoding is randomly assigned to the node representation, while the edge encoding is calculated based on the start node encoding and the end node encoding.

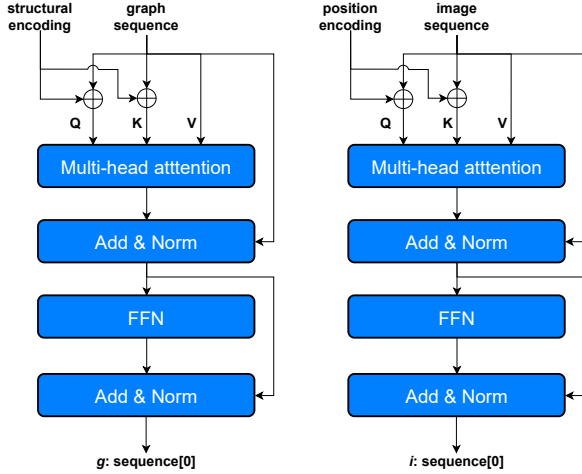


Figure 11: Architecture of the graph Transformer and the image Transformer. The learnable graph embedding in the graph sequence from the last encoder layer is adopted as the final scene graph representation. This is also for images.

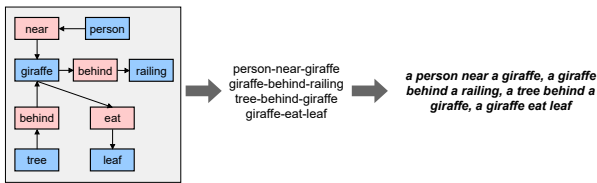


Figure 12: To convert the location-free scene graph into a sentence that can be used as a query for image retrieval, we combine the triplets within the scene graph and incorporate indefinite articles to specify the entities.

and images in the test set is 0.50/0.55. The qualitative results for similarity calculation are shown in Fig. 13 (using

Layer Number	Graph	Image	R-Precision (LF Graph) K=50	R-Precision (LF Graph) K=100	R-Precision (LB Graph) K=50	R-Precision (LB Graph) K=100	params (M)
4	4	4	65.7	54.9	76.1	66.5	41.2/41.3
4	6	6	67.5	57.3	78.2	69.4	45.4/45.5
6	4	4	67.2	56.5	78.3	70.4	45.4/45.5
6	6	6	67.9	58.0	78.9	71.0	49.6/49.7
6	8	8	68.0	58.3	78.3	70.1	53.8/53.9
8	6	6	67.6	57.1	78.4	69.7	53.8/53.9
8	8	8	67.1	56.3	78.0	69.2	58.0/58.1

Table 5: Ablation study for the Transformer layer number. Finally, we adopt a layer number of 6 for both the graph Transformer and the image Transformer. For parameters, the left numbers are for location-free scene graphs, while the right numbers are for location-bound scene graphs.

location-free scene graphs) and in Fig. 14 (using location-bound scene graphs). For the Open Images V6 dataset, the maximum similarity between any location-free/location-bound scene graph and image in the test set is 0.83/0.76 and the minimum is -0.58/-0.53, while the average similarity between matched ground truth scene graphs and images in the test set is 0.56/0.56. The qualitative results are shown in Fig. 15 (using location-free scene graphs) and in Fig. 16 (using location-bound scene graphs).

C. Additional Ablation Study

We conduct experiments on the Visual Genome dataset to verify the impact of different layer numbers on the performance of the graph Transformer and the image Transformer. The results are presented in Table 5.

For location-free scene graphs, when both the graph Transformer and the image Transformer have 4 layers, the R-precision score (K= 100) is 54.9. For location-bound scene graphs, the score is 66.5. As we increase the number of layers in both Transformers, the model performance

improves due to the increased number of parameters. The best performance is achieved when both Transformers have 6 layers. However, increasing the number of layers to 8 leads to a drop in performance. We conjecture that this may be caused by overfitting.

D. Additional Results for Image Retrieval

We use location-free scene graphs, and location-bound scene graphs as queries to retrieve the matching image from 100 image candidates on the Visual Genome dataset. The query scene graph and the image candidates are encoded, and the similarity between the scene graph and images is computed. The candidate with the highest similarity is viewed as the matched image. For comparison, we also use CLIP to retrieve the image that match the text. The qualitative results using the text and location-free scene graph are presented in Fig. 17, and the qualitative results using location-bound scene graphs are presented in Fig. 18. We show the five images with the highest similarity and the five images with the lowest. The image corresponding to the input query in the ground truth is highlighted in green. Due to the large number of image candidates, some scenes similar to those described in the scene graph appear in the top five images.

References

- [1] Oron Ashual and Lior Wolf. Specifying object attributes and relations in interactive scene generation. In *Proceedings of the IEEE/CVF international conference on computer vision*, pages 4561–4569, 2019. 2
- [2] Nicolas Carion, Francisco Massa, Gabriel Synnaeve, Nicolas Usunier, Alexander Kirillov, and Sergey Zagoruyko. End-to-end object detection with transformers. In *Computer Vision—ECCV 2020: 16th European Conference, Glasgow, UK, August 23–28, 2020, Proceedings, Part I 16*, pages 213–229. Springer, 2020. 4
- [3] Xinlei Chen, Hao Fang, Tsung-Yi Lin, Ramakrishna Vedantam, Saurabh Gupta, Piotr Dollár, and C Lawrence Zitnick. Microsoft coco captions: Data collection and evaluation server. *arXiv preprint arXiv:1504.00325*, 2015. 2
- [4] Meng-Jiun Chiou, Henghui Ding, Hanshu Yan, Changhu Wang, Roger Zimmermann, and Jiashi Feng. Recovering the unbiased scene graphs from the biased ones. In *Proceedings of the 29th ACM International Conference on Multimedia*, pages 1581–1590, 2021. 1
- [5] Yuren Cong, Hanno Ackermann, Wentong Liao, Michael Ying Yang, and Bodo Rosenhahn. Nodis: Neural ordinary differential scene understanding. In *Computer Vision—ECCV 2020: 16th European Conference, Glasgow, UK, August 23–28, 2020, Proceedings, Part XX 16*, pages 636–653. Springer, 2020. 1, 6
- [6] Yuren Cong, Michael Ying Yang, and Bodo Rosenhahn. Reltr: Relation transformer for scene graph generation. *arXiv preprint arXiv:2201.11460*, 2022. 6, 7
- [7] Karan Desai and Justin Johnson. Virtex: Learning visual representations from textual annotations. In *Proceedings of the IEEE/CVF conference on computer vision and pattern recognition*, pages 11162–11173, 2021. 2
- [8] Jacob Devlin, Ming-Wei Chang, Kenton Lee, and Kristina Toutanova. Bert: Pre-training of deep bidirectional transformers for language understanding. *arXiv preprint arXiv:1810.04805*, 2018. 4
- [9] Naina Dhir, Florian Ritter, and Andreas Kunz. Bgt-net: Bidirectional gru transformer network for scene graph generation. In *Proceedings of the IEEE/CVF Conference on Computer Vision and Pattern Recognition*, pages 2150–2159, 2021. 2
- [10] Lizhao Gao, Bo Wang, and Wenmin Wang. Image captioning with scene-graph based semantic concepts. In *Proceedings of the 2018 10th international conference on machine learning and computing*, pages 225–229, 2018. 1
- [11] Jiuxiang Gu, Handong Zhao, Zhe Lin, Sheng Li, Jianfei Cai, and Mingyang Ling. Scene graph generation with external knowledge and image reconstruction. In *Proceedings of the IEEE/CVF conference on computer vision and pattern recognition*, pages 1969–1978, 2019. 2
- [12] Kaiming He, Xiangyu Zhang, Shaoqing Ren, and Jian Sun. Deep residual learning for image recognition. In *Proceedings of the IEEE conference on computer vision and pattern recognition*, pages 770–778, 2016. 4
- [13] Roei Herzig, Amir Bar, Huijuan Xu, Gal Chechik, Trevor Darrell, and Amir Globerson. Learning canonical representations for scene graph to image generation. In *Computer Vision—ECCV 2020: 16th European Conference, Glasgow, UK, August 23–28, 2020, Proceedings, Part XXVI 16*, pages 210–227. Springer, 2020. 1, 2, 3
- [14] Marcel Hildebrandt, Hang Li, Rajat Koner, Volker Tresp, and Stephan Günnemann. Scene graph reasoning for visual question answering. *arXiv preprint arXiv:2007.01072*, 2020. 1, 2
- [15] Ashish Jaiswal, Ashwin Ramesh Babu, Mohammad Zaki Zadeh, Debapriya Banerjee, and Fillia Makedon. A survey on contrastive self-supervised learning. *Technologies*, 9(1):2, 2020. 2
- [16] Jingwei Ji, Ranjay Krishna, Li Fei-Fei, and Juan Carlos Niebles. Action genome: Actions as compositions of spatio-temporal scene graphs. In *Conference on Computer Vision and Pattern Recognition*, pages 10236–10247, 2020. 2
- [17] Justin Johnson, Agrim Gupta, and Li Fei-Fei. Image generation from scene graphs. In *Proceedings of the IEEE conference on computer vision and pattern recognition*, pages 1219–1228, 2018. 1, 2
- [18] Justin Johnson, Ranjay Krishna, Michael Stark, Li-Jia Li, David Shamma, Michael Bernstein, and Li Fei-Fei. Image retrieval using scene graphs. In *Proceedings of the IEEE conference on computer vision and pattern recognition*, pages 3668–3678, 2015. 1, 2, 7
- [19] Thomas N Kipf and Max Welling. Semi-supervised classification with graph convolutional networks. *arXiv preprint arXiv:1609.02907*, 2016. 3, 8

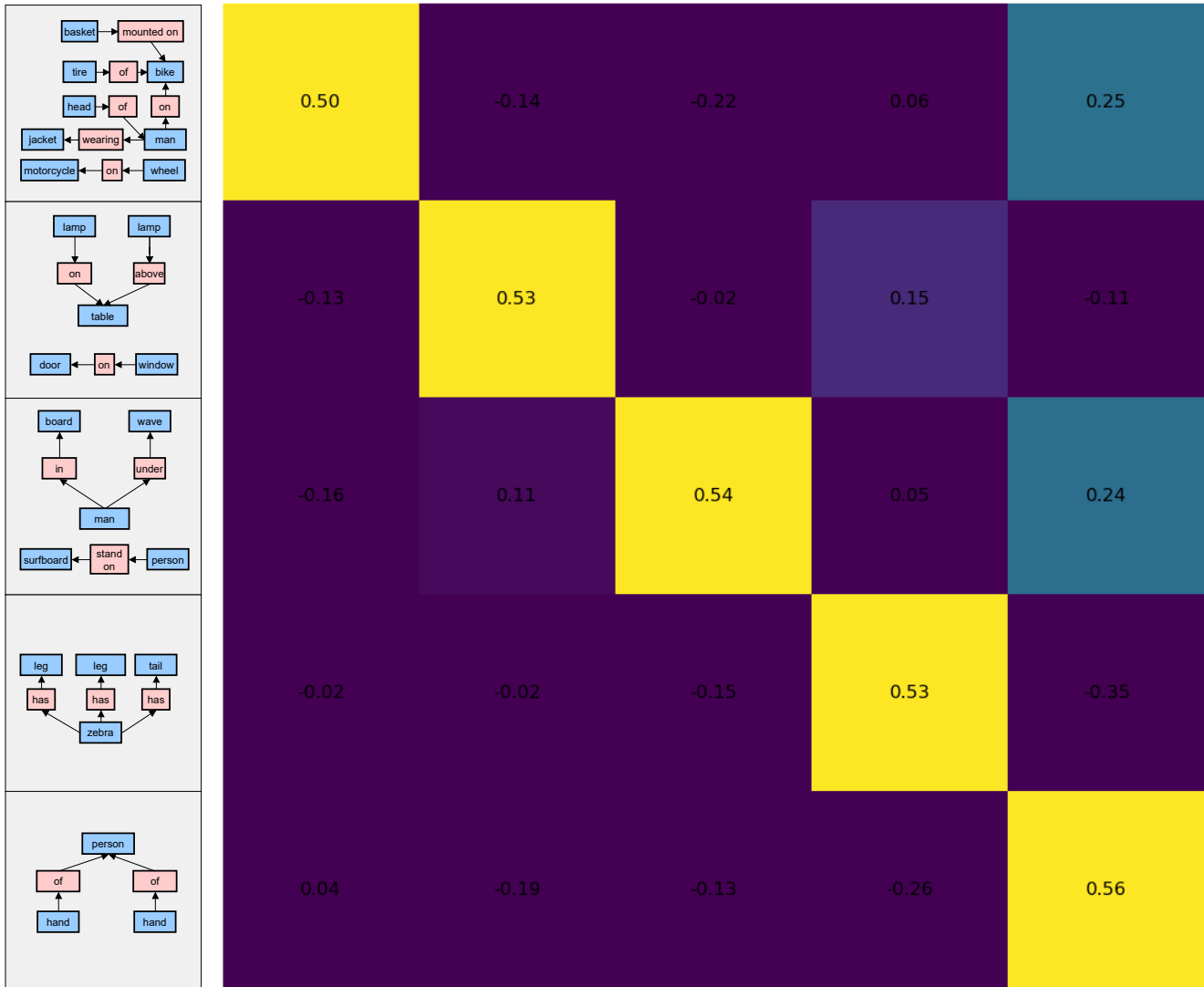


Figure 13: Qualitative results of similarity between location-free scene graphs and images for the Visual Genome dataset. For better visualization, the images are resized.

[20] Ranjay Krishna, Yuke Zhu, Oliver Groth, Justin Johnson, Kenji Hata, Joshua Kravitz, Stephanie Chen, Yannis Kalantidis, Li-Jia Li, David A Shamma, et al. Visual genome: Connecting language and vision using crowdsourced dense image annotations. *International journal of computer vision*, 123:32–73, 2017. 2, 5, 9

[21] Alina Kuznetsova, Hassan Rom, Neil Alldrin, Jasper Uijlings, Ivan Krasin, Jordi Pont-Tuset, Shahab Kamali, Stefan

Popov, Matteo Mallocci, Alexander Kolesnikov, et al. The open images dataset v4: Unified image classification, object detection, and visual relationship detection at scale. *International Journal of Computer Vision*, 128(7):1956–1981, 2020. 2, 5, 9

[22] Soohyeong Lee, Ju-Whan Kim, Youngmin Oh, and Joo Hyuk Jeon. Visual question answering over scene graph. In *2019 First International Conference on Graph Computing*

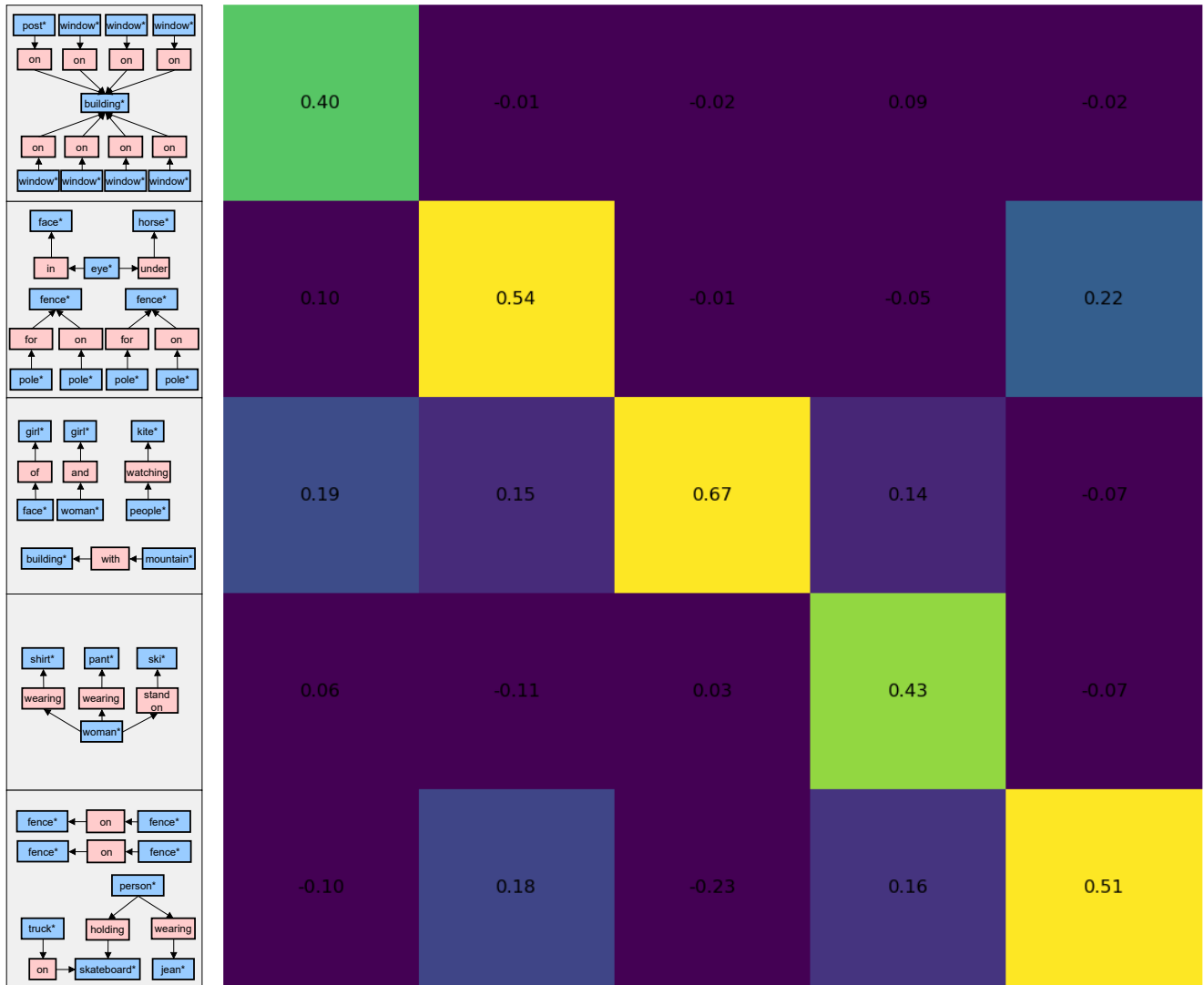


Figure 14: Qualitative results of similarity between location-bound scene graphs and images for the Visual Genome dataset. For better visualization, the images are resized. *entity** indicates the bounding box is given in the location-bound scene graph.

(GC), pages 45–50. IEEE, 2019. 1, 2

- [23] Lin Li, Long Chen, Yifeng Huang, Zhimeng Zhang, Songyang Zhang, and Jun Xiao. The devil is in the labels: Noisy label correction for robust scene graph generation. In *Proceedings of the IEEE/CVF Conference on Computer Vision and Pattern Recognition*, pages 18869–18878, 2022. 2
- [24] Rongjie Li, Songyang Zhang, and Xuming He. Sgr: End-to-end scene graph generation with transformer. In *Proceedings*

of the IEEE/CVF Conference on Computer Vision and Pattern Recognition, pages 19486–19496, 2022. 6, 7

- [25] Rongjie Li, Songyang Zhang, Bo Wan, and Xuming He. Bipartite graph network with adaptive message passing for unbiased scene graph generation. In *Proceedings of the IEEE/CVF Conference on Computer Vision and Pattern Recognition*, pages 11109–11119, 2021. 1, 6, 7
- [26] Yikang Li, Tao Ma, Yeqi Bai, Nan Duan, Sining Wei, and



Figure 15: Qualitative results of similarity between location-free scene graphs and images for the Open Images V6 dataset. For better visualization, the images are resized.

Xiaogang Wang. Pastegan: A semi-parametric method to generate image from scene graph. *Advances in Neural Information Processing Systems*, 32, 2019. 1, 2, 3

[27] Xin Lin, Changxing Ding, Jinquan Zeng, and Dacheng Tao. Gps-net: Graph property sensing network for scene graph generation. In *Proceedings of the IEEE/CVF Conference on Computer Vision and Pattern Recognition*, pages 3746–3753, 2020. 1

[28] Hengyue Liu, Ning Yan, Masood Mortazavi, and Bir Bhanu. Fully convolutional scene graph generation. In *Proceedings of the IEEE/CVF Conference on Computer Vision and Pattern Recognition*, pages 11546–11556, 2021. 6

[29] Ilya Loshchilov and Frank Hutter. Decoupled weight decay regularization. *arXiv preprint arXiv:1711.05101*, 2017. 5

[30] Cewu Lu, Ranjay Krishna, Michael Bernstein, and Li Fei-Fei. Visual relationship detection with language priors. In

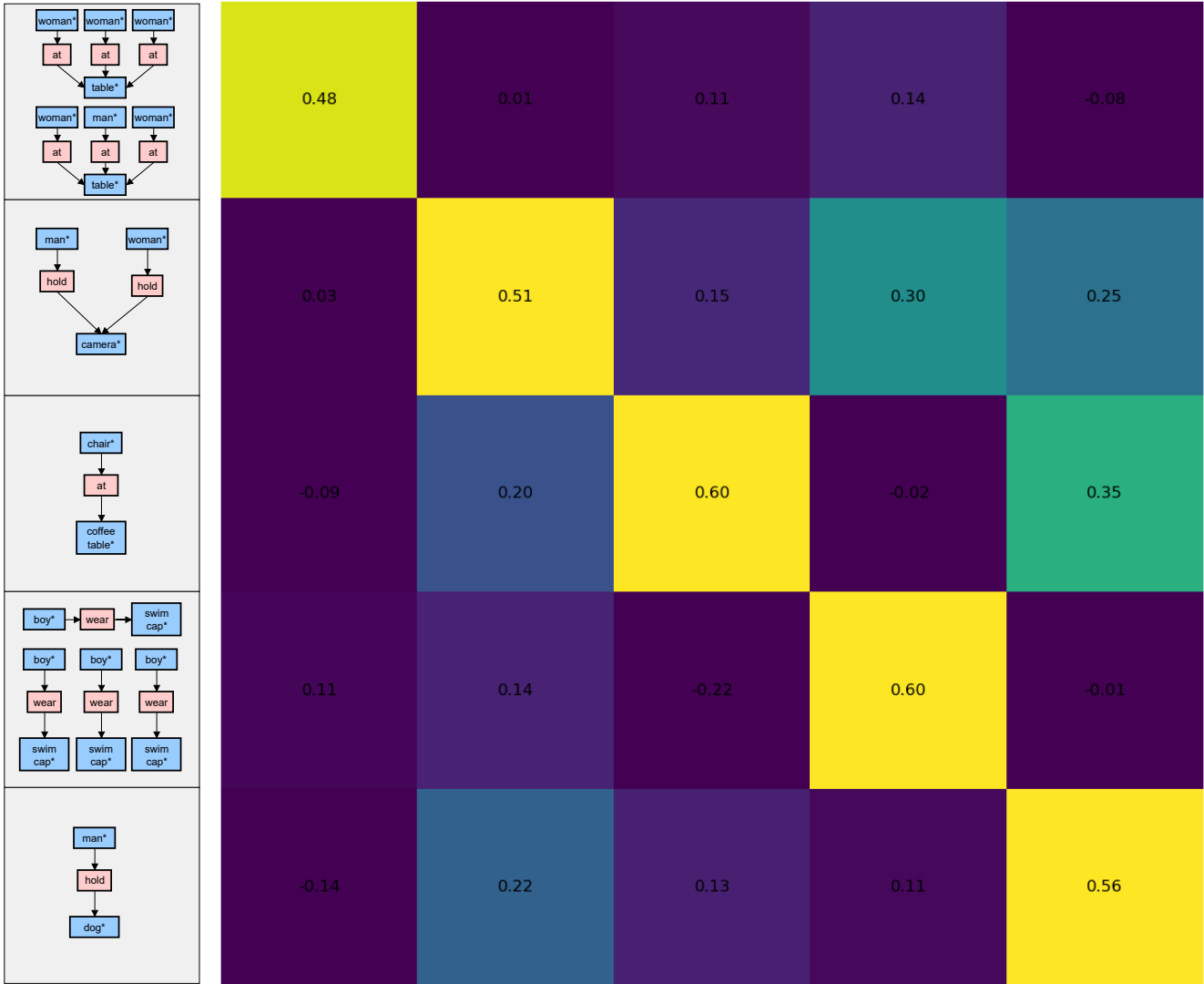


Figure 16: Qualitative results of similarity between location-bound scene graphs and images for the Open Images V6 dataset. For better visualization, the images are resized. *entity** indicates the bounding box is given in the location-bound scene graph.

Computer Vision–ECCV 2016: 14th European Conference, Amsterdam, The Netherlands, October 11–14, 2016, Proceedings, Part I 14, pages 852–869. Springer, 2016. 2, 5

[31] Yichao Lu, Himanshu Rai, Jason Chang, Boris Knyazev, Guangwei Yu, Shashank Shekhar, Graham W Taylor, and Maksims Volkovs. Context-aware scene graph generation with seq2seq transformers. In *Proceedings of the IEEE/CVF international conference on computer vision*, pages 15931–

15941, 2021. 2

[32] Brian McFee, Gert Lanckriet, and Tony Jebara. Learning multi-modal similarity. *Journal of machine learning research*, 12(2), 2011. 2

[33] Dong Huk Park, Samaneh Azadi, Xihui Liu, Trevor Darrell, and Anna Rohrbach. Benchmark for compositional text-to-image synthesis. In *Thirty-fifth Conference on Neural Information Processing Systems Datasets and Benchmarks Track*



Figure 17: Qualitative results for image retrieval using the text (first row) and location-free scene graph (second row) as queries. The five images with the highest similarity and the five images with the lowest similarity from 100 image candidates are shown. The corresponding image to the query is highlighted in green. CLIP cannot retrieve the correct image, while our framework assigns the highest similarity score to the matched image, indicating its effectiveness in image retrieval.



Figure 18: Qualitative results for image retrieval using location-bound scene graphs as queries. The five images with the highest similarity and the five images with the lowest similarity from 100 image candidates are shown. The images corresponding to the scene graphs in the ground truth are highlighted in green. *entity** indicates the bounding box is given in the location-bound scene graph.

(Round 1), 2021. 2

[34] Alec Radford, Jong Wook Kim, Chris Hallacy, Aditya Ramesh, Gabriel Goh, Sandhini Agarwal, Girish Sastry, Amanda Askell, Pamela Mishkin, Jack Clark, et al. Learning transferable visual models from natural language supervision. In *International conference on machine learning*, pages 8748–8763. PMLR, 2021. 2, 7, 9

[35] Brigit Schroeder and Subarna Tripathi. Structured query-based image retrieval using scene graphs. In *Proceedings of the IEEE/CVF Conference on Computer Vision and Pattern*

Recognition Workshops, pages 178–179, 2020. 1, 7

[36] Jiaxin Shi, Hanwang Zhang, and Juanzi Li. Explainable and explicit visual reasoning over scene graphs. In *Proceedings of the IEEE/CVF conference on computer vision and pattern recognition*, pages 8376–8384, 2019. 1, 2

[37] Mohammed Suhail, Abhay Mittal, Behjat Siddiquie, Chris Broaddus, Jayan Eledath, Gerard Medioni, and Leonid Sigal. Energy-based learning for scene graph generation. In *Proceedings of the IEEE/CVF conference on computer vision and pattern recognition*, pages 13936–13945, 2021. 6

- [38] Kaihua Tang, Yulei Niu, Jianqiang Huang, Jiaxin Shi, and Hanwang Zhang. Unbiased scene graph generation from biased training. In *Proceedings of the IEEE/CVF conference on computer vision and pattern recognition*, pages 3716–3725, 2020. [1](#), [6](#)
- [39] Kaihua Tang, Hanwang Zhang, Baoyuan Wu, Wenhan Luo, and Wei Liu. Learning to compose dynamic tree structures for visual contexts. In *Proceedings of the IEEE/CVF conference on computer vision and pattern recognition*, pages 6619–6628, 2019. [5](#)
- [40] Yao Teng and Limin Wang. Structured sparse r-cnn for direct scene graph generation. In *Proceedings of the IEEE/CVF Conference on Computer Vision and Pattern Recognition*, pages 19437–19446, 2022. [6](#), [7](#)
- [41] Ashish Vaswani, Noam Shazeer, Niki Parmar, Jakob Uszkoreit, Llion Jones, Aidan N Gomez, Łukasz Kaiser, and Illia Polosukhin. Attention is all you need. In *Advances in neural information processing systems*, volume 30, 2017. [2](#), [3](#), [4](#), [9](#)
- [42] Sijin Wang, Ruiping Wang, Ziwei Yao, Shiguang Shan, and Xilin Chen. Cross-modal scene graph matching for relationship-aware image-text retrieval. In *Proceedings of the IEEE/CVF Winter Conference on Applications of Computer Vision (WACV)*, March 2020. [1](#), [3](#)
- [43] Danfei Xu, Yuke Zhu, Christopher B Choy, and Li Fei-Fei. Scene graph generation by iterative message passing. In *Proceedings of the IEEE conference on computer vision and pattern recognition*, pages 5410–5419, 2017. [2](#), [5](#)
- [44] Tao Xu, Pengchuan Zhang, Qiuyuan Huang, Han Zhang, Zhe Gan, Xiaolei Huang, and Xiaodong He. Attngan: Fine-grained text to image generation with attentional generative adversarial networks. In *Proceedings of the IEEE Conference on Computer Vision and Pattern Recognition (CVPR)*, June 2018. [2](#)
- [45] Shaotian Yan, Chen Shen, Zhongming Jin, Jianqiang Huang, Rongxin Jiang, Yaowu Chen, and Xian-Sheng Hua. Pcp1: Predicate-correlation perception learning for unbiased scene graph generation. In *Proceedings of the 28th ACM International Conference on Multimedia*, pages 265–273, 2020. [1](#)
- [46] Jianwei Yang, Jiasen Lu, Stefan Lee, Dhruv Batra, and Devi Parikh. Graph r-cnn for scene graph generation. In *Proceedings of the European conference on computer vision (ECCV)*, pages 670–685, 2018. [2](#)
- [47] Ling Yang, Zhilin Huang, Yang Song, Shenda Hong, Guohao Li, Wentao Zhang, Bin Cui, Bernard Ghanem, and Ming-Hsuan Yang. Diffusion-based scene graph to image generation with masked contrastive pre-training. *arXiv preprint arXiv:2211.11138*, 2022. [1](#), [2](#), [3](#)
- [48] Michael Ying Yang, Wentong Liao, Hanno Ackermann, and Bodo Rosenhahn. On support relations and semantic scene graphs. *ISPRS journal of photogrammetry and remote sensing*, 131:15–25, 2017. [1](#)
- [49] Xu Yang, Kaihua Tang, Hanwang Zhang, and Jianfei Cai. Auto-encoding scene graphs for image captioning. In *Proceedings of the IEEE/CVF conference on computer vision and pattern recognition*, pages 10685–10694, 2019. [1](#), [2](#)
- [50] Sangwoong Yoon, Woo Young Kang, Sungwook Jeon, SeongEun Lee, Changjin Han, Jonghun Park, and Eun-Sol Kim. Image-to-image retrieval by learning similarity between scene graphs. In *Proceedings of the AAAI Conference on Artificial Intelligence*, volume 35, pages 10718–10726, 2021. [1](#), [2](#)
- [51] Rowan Zellers, Mark Yatskar, Sam Thomson, and Yejin Choi. Neural motifs: Scene graph parsing with global context. In *Proceedings of the IEEE conference on computer vision and pattern recognition*, pages 5831–5840, 2018. [1](#), [2](#), [6](#)
- [52] Ji Zhang, Kevin J Shih, Ahmed Elgammal, Andrew Tao, and Bryan Catanzaro. Graphical contrastive losses for scene graph parsing. In *Proceedings of the IEEE/CVF Conference on Computer Vision and Pattern Recognition*, pages 11535–11543, 2019. [3](#), [5](#), [6](#)
- [53] Yuhao Zhang, Hang Jiang, Yasuhide Miura, Christopher D Manning, and Curtis P Langlotz. Contrastive learning of medical visual representations from paired images and text. In *Machine Learning for Healthcare Conference*, pages 2–25. PMLR, 2022. [2](#)